

# Fourier spectral method for higher order space fractional reaction-diffusion equations\*

Edson Pindza<sup>†</sup>, Kolade M. Owolabi<sup>‡</sup>

<sup>†</sup>Department of Mathematics and Applied Mathematics, University of Pretoria Pretoria 002,  
South Africa

<sup>‡</sup>Department of Mathematical Sciences, Federal University of Technology, PMB 704, Akure,  
Ondo State, Nigeria

## Abstract

Evolution equations containing fractional derivatives can provide suitable mathematical models for describing important physical phenomena. In this paper, we propose a fast and accurate method for numerical solutions of space fractional reaction-diffusion equations. The proposed method is based on an exponential integrator scheme in time and the Fourier spectral method in space. The main advantages of this method are that it yields a fully diagonal representation of the fractional operator, with increased accuracy and efficiency, and a completely straightforward extension to high spatial dimensions. Although, in general, it is not obvious what role a high fractional derivative can play and how to make use of arbitrarily high-order fractional derivatives, we introduce them to describe fractional hyper-diffusions in reaction diffusion. The scheme justified by a number of computational experiments, this includes two and three dimensional partial differential equations. Numerical experiments are provided to validate the effectiveness of the proposed approach.

2010 Mathematics Subject Classification: 35A05, 35K57, 65L05, 65M06, 93C10

**Keywords:** Fractional exponential integrators; Fourier transform; Fractional reaction-diffusion system; Pattern formation; Turing instability.

## 1 Introduction

The subject of fractional calculus has gained considerable popularity and importance during the past three decades or so, due mainly to its demonstrated applications in numerous seemingly diverse and widespread fields of science and engineering [1]. It does indeed provide several potentially useful tools for solving differential and integral equations, and various other problems involving special functions of mathematical physics as well as their extensions and generalizations in one and more variables.

---

<sup>†</sup>E-mail addresses: pindzaedson@yahoo.fr (E. Pindza); mkowolax@yahoo.com (K.M. Owolabi)

The first and exclusive study of the fractional calculus subject is dated to 1974 in the classical fractional calculus book by Oldham and Spanier [2] that was published in 1974. Years later, Podlubny [3] published a book on fractional calculus, which deals principally with fractional differential equations. Later, some researchers work especially on fractional models of anomalous kinetics of complex processes [4, 5, 6]. Operators of fractional integrals and fractional derivatives, which are based essentially upon the familiar Cauchy-Goursat Integral Formula. In recent years, many authors have demonstrated the usefulness of such types of fractional calculus operators in obtaining particular solutions of numerous families of homogeneous, as well as nonhomogeneous, ordinary and partial differential equations which are associated with many of the celebrated equations of mathematical physics [1]

In recent years, evolution equations containing fractional derivatives are becoming increasingly used as a powerful modelling approach for understanding the many aspects of nonlocality and spatial heterogeneity. Recently, great interests have been witnessed in fractional calculus modeling in many fields of science and engineering, from geophysics to biology. Fractional derivatives extend the concept of ordinary derivatives and serve as a good tool for taking into account memory mechanism in the random walk and anomalous diffusion in physical problems [7, 8]. Fractional derivative has found its success in physical and biological modeling [9, 10], financial analysis [11], and image processing [12].

However, the numerical approximation of these models is computationally demanding and imposes a number of computational constraints. In recent years, various methods have been devised to find the exact and approximate solutions of fractional partial differential equations (FPDEs) [13, 14] in order to provide more information for understanding physical phenomena arising in numerous scientific and engineering fields. Keskin and Oturanc [15] proposed a semi analytical method, the reduced differential transform method (RDTM) for the fractional differential equations. Lui *et al.* [16] derived the solution of time fractional advection-dispersion equation using variable transformation, Mellin and Laplace transforms, and properties of H-functions. Lin and Xu [17] combined finite difference and spectral approximations to solve numerically time-fractional diffusion equations. In this paper, a fast Fourier transform (FFT) is proposed to numerically integrate the high-order fractional PDEs so as to avoid stringent stability constraints in solving high-order evolution PDEs. The spatial discretisation results into a system of fractional ordinary differential equations in Fourier space that are solved using fractional exponential time integrators.

We mainly study models arising in the application areas of theoretical biology, ecology and chemistry, modelled by some time-space fractional reaction-diffusion system of equations

$$\frac{\partial U_i(X, t)}{\partial X} = -K_i (-\Delta^{\alpha/2}) U_i(X, t) + f(U_i, t), \quad 0 < \alpha \leq \infty, \quad (1)$$

where  $\alpha$  is a parameter describing the order of the fractional space fractional Laplacian operator in the Caputo sense, respectively, and  $f(U_i, t)$  is the reaction term. The system (1) is subjected to some initial condition  $U_i(X, 0) = U_{i,0}(X)$  and homogeneous Neumann boundary conditions  $\frac{\partial U_i}{\partial X} = 0$ . The parameters  $K_i, i = 1, 2 \in \mathbb{R}_+$  are diffusion coefficients. The operator  $(-\Delta)^{\alpha/2}$  denote the fractional time derivative and the fractional Laplacian operator. The function  $U_i(X, t)$  is assumed to be a causal function of time, i.e., vanishing for  $t < 0$ . The general response expression contains parameters describing the order of the fractional derivatives that can be varied to obtain various responses.

There are several definitions of a fractional derivative of order  $q > 0$  [3]. The two most

commonly used definitions are the Riemann-Liouville and Caputo. The Riemann-Liouville fractional integration of order  $q$  is defined as

$$J_a^q f(x) = \frac{1}{\Gamma(q)} \int_a^x (x - \xi)^{q-1} f(\xi) d\xi, \quad q > 0, \quad x > 0. \quad (2)$$

The next two equations define Riemann-Liouville and Caputo fractional derivatives of order  $q$ , respectively,

$$D_a^q f(x) = \frac{d^m}{dx^m} (J_a^{m-q} f(x)), \quad (3)$$

$$D_{*a}^q f(x) = J_a^{m-q} \left( \frac{d^m}{dx^m} f(x) \right), \quad (4)$$

where  $m - 1 < q \leq m$  and  $m \in \mathbb{N}$ . For now, the Caputo fractional derivative will be denoted by  $D_{*a}^q$  to maintain a clear distinction with the Riemann-Liouville fractional derivative. The Caputo fractional derivative is considered here because it allows traditional initial and boundary conditions to be included in the formulation of the problem.

This paper is organized as follows. In Section 2, we introduce some general definitions of fractional derivatives. In Section 3, we explore mathematical analysis of coupled systems of chemical reaction, the main focus will be on the Schnakenberg and Gray-Scott systems. A robust numerical method based on Fourier transform method and the exponential integrator scheme of Runge-Kutta type designed for the solution of the fractional chemical reaction-diffusion system is formulated and discussed in Section 4. The suitability and applicability of the numerical method formulated and tested in Section 5. The paper ends with concluding remarks and scope for future research in Section 6.

## 2 Basics of fractional calculus

There are several definitions of a fractional derivative of order  $\alpha > 0$ , for instance, Riemann-Liouville, Caputo Riesz and Jumarie's fractional derivative [3]. Here, some basic definitions and properties of the fractional calculus theory which can be used in this paper are presented.

**Definition 2.1.** A real function  $f(x); x > 0$ , is said to be in the space  $C_\nu$ ,  $\nu \in \mathbb{R}$  if there exists a real number  $p > \nu$  such that  $f(x) = x^p f_1(x)$ , where  $f_1(x) \in [0, \infty)$ . Clearly  $C_\nu \subset C_\beta$  if  $\beta \leq \nu$ .

**Definition 2.2.** A function  $f(x)$ ,  $x > 0$ , is said to be in the space  $C_\nu^m$ ,  $m \in \mathbb{N} \cup \{0\}$ , if  $f^{(m)} \in C_\nu$ .

**Definition 2.3.** Let  $f \in C_q^m$ ,  $m \in \mathbb{N}$ . The Caputo fractional derivative operator of order  $p > 0$  is defined as [3]:

$${}_a D_t^q f(t) = \begin{cases} \frac{1}{\Gamma(m-q)} \int_a^t (t-\tau)^{m-q-1} \frac{d^m f(\tau)}{d\tau^m} d\tau, & m-1 < q < m, \\ \frac{d^m f(\tau)}{d\tau^m}, & q = m \in \mathbb{N} \end{cases} \quad (5)$$

where,  $m$  is the smallest integer larger than the parameter  $q$ ,  $q$  is the order of the derivative and is allowed to be real or even complex,  $a$  is the initial value of function  $f$ . In the present work only real and positive values of  $q$  are considered. For the Caputo's derivative we have

$${}_t D_b^q f(t) = \begin{cases} \frac{1}{\Gamma(m-q)} \int_b^t (t-\tau)^{m-q-1} \frac{d^m f(\tau)}{d\tau^m} d\tau, & m-1 < q < m, \\ \frac{d^m f(\tau)}{d\tau^m}, & q = m \in \mathbb{N} \end{cases} \quad (6)$$

**Definition 2.4.** The left sided Riemann-Liouville fractional differential equation of order  $q \geq 0$ , of a function  $f \in C_q^m$  on  $(a, \infty)$ , is defined as [3]:

$${}_a D_t^q f(t) = \begin{cases} \frac{1}{\Gamma(m-q)} \frac{d^m}{dt^m} \left( \int_a^t (t-\tau)^{q-1} f(\tau) d\tau \right), & m-1 < q < m, \\ f(x) & q = 0 \\ \frac{d^m f(\tau)}{d\tau^m}, & q = m \in \mathbb{N} \end{cases} \quad (7)$$

where  $\Gamma$  denotes the Euler Gamma function defined by

$$\Gamma(z) = \int_0^\infty t^{z-1} e^{-t} dt. \quad (8)$$

Analogously for  $f \in C_q^m$  on  $(-\infty, b)$ , we have

$${}_t D_b^q f(t) = \begin{cases} \frac{1}{\Gamma(m-q)} \frac{d^m}{dt^m} \left( \int_t^b (t-\tau)^{q-1} f(\tau) d\tau \right), & m-1 < q < m, \\ f(x) & q = 0 \\ \frac{d^m f(\tau)}{d\tau^m}, & q = m \in \mathbb{N} \end{cases} \quad (9)$$

For a wide class of functions, the Grünwald-Letnikov and the Riemann-Liouville definitions are equivalent [3].

Primarily, the Caputo fractional differential equation computes an ordinary differential equation, followed by a fractional integral to achieve the desired order of fractional derivative, and then the Riemann-Liouville fractional differential equation is computed in the reverse order. The Caputo fractional differential equation allows traditional initial and boundary conditions to be included in the formulation of the problem, but for homogeneous initial condition assumption, these two operators coincide. For more details on the geometric and physical interpretation for fractional differential equations of both the Riemann-Liouville and Caputo types, see [3].

### 3 Mathematical analysis of the main equations

Our main focus in this section is to find necessary and sufficient conditions for the diffusion-driven instability associated with the homogeneous steady state of two variable chemical species, such as the Schnakenberg and Gray-Scott systems. We would also investigate how a

spatial pattern can evolve in such dynamical systems. We let  $u$  and  $v$  be the variables that represent the two chemical species. We assume  $u(\mathbf{X}, 0)$ ,  $v(\mathbf{X}, 0)$  to be their respective initial conditions. Since patterns are evolved only by self-organization, not with external input, hence, zero-flux boundary conditions are chosen in the form

$$(\nu \cdot \nabla) \begin{pmatrix} u \\ v \end{pmatrix} = 0 \quad (10)$$

where  $\nu$  is the outer normal to the closed boundary  $\partial\Omega$ . In the presence of small perturbation, we consider the homogeneous steady state  $(u^*, v^*)$  which corresponds to solution

$$\mathcal{F}(u, v) = 0, \quad \mathcal{G}(u, v) = 0.$$

The aim is to examine linear instability of the homogeneous steady state expected to be linearly stable in absence of diffusion. The spatially homogeneous system become

$$\begin{aligned} \frac{du}{dt} &= \gamma \mathcal{F}(u, v) = 0, \\ \frac{dv}{dt} &= \gamma \mathcal{G}(u, v) = 0, \end{aligned} \quad (11)$$

To see how the kinetics (11) behave, we linearized around the steady state  $(u^*, v^*)$  and let  $\mathcal{W} = (u - u^*, v - v^*)$ , to obtain the system

$$\frac{d\mathcal{W}}{dt} = \gamma \mathbf{A} \mathcal{W}, \quad (12)$$

where

$$\mathbf{A} = \begin{pmatrix} \mathcal{F}_u & \mathcal{F}_v \\ \mathcal{G}_u & \mathcal{G}_v \end{pmatrix}_{(u^*, v^*)}$$

is the Jacobian of the kinetics. Next, from the knowledge of ODE we seek solutions  $\mathcal{W}$  which are proportional to  $e^{\lambda t}$ , where  $\lambda$  is an eigenvalue of the Jacobian. The eigenvalue problem  $(\gamma \mathbf{A} - \lambda \mathbf{I}) \mathcal{W} = 0$  of the homogeneous steady state  $\mathcal{W} = 0$  is stable when  $Re\lambda < 0$ . That is,

$$\lambda^2 - \gamma(\mathcal{F}_u + \mathcal{G}_v)\lambda + \gamma^2(\mathcal{F}_u\mathcal{G}_v) + \gamma^2(\mathcal{F}_u\mathcal{G}_v - \mathcal{F}_v\mathcal{G}_u) = 0, \quad (13)$$

which on simplification yields

$$\lambda_{1,2} = \frac{\gamma \left[ (\mathcal{F}_u + \mathcal{G}_v) \pm \sqrt{(\mathcal{F}_u + \mathcal{G}_v)^2 - 4(\mathcal{F}_u\mathcal{G}_v - \mathcal{F}_v\mathcal{G}_u)} \right]}{2}$$

where  $tr\mathbf{A} = \mathcal{F}_u + \mathcal{G}_v$  and  $det\mathbf{A} = \mathcal{F}_u\mathcal{G}_v - \mathcal{F}_v\mathcal{G}_u$ . Thus, stability conditions of the time-dependent problem are satisfied if

$$tr\mathbf{A} < 0 \quad \text{and} \quad det\mathbf{A} > 0. \quad (14)$$

In what follows, we shall examine quickly the homogeneous stability conditions and diffusion-driven instability for the two notable examples we are considering in this paper.

### 3.1 Schnakenberg system

The dynamical model (11) can be written in the form of a reaction-diffusion system

$$\begin{aligned} u_t &= \nabla u + \gamma \mathcal{F}(u, v) \text{ in } \Omega, \\ v_t &= d \nabla v + \gamma \mathcal{G}(u, v) \text{ in } \Omega, \end{aligned} \quad (15)$$

subject to homogeneous Neumann boundary conditions, where  $\gamma$  and  $d = D_u/D_v$  are positive constants modeling the effect of domain size and the ratio of diffusion coefficients, respectively.  $u$  and  $v$  remain the chemical species,  $\nabla u$  and  $d \nabla v$  are the diffusive terms. If the reaction (reagent) terms  $\mathcal{F}(u, v) = (a - u + u^2v)$  and  $\mathcal{G}(u, v) = (b - u^2v)$ , reaction-diffusion system (15) is known as the Schnakenberg model [18, 19]. The parameter  $\gamma$  is treated as dimensionless constant (expected to be a key parameter),  $a$  and  $b$  are positive parameters.

From already well-known results, without the presence of the diffusive terms, the stationary state for the Schnakenberg system exists when

$$\mathcal{F}(u^*, v^*) = \gamma(a - u^* + u^{*2}v^*) = 0, \quad \mathcal{G}(u^*, v^*) = \gamma(b - u^{*2}v^*) = 0.$$

On setting  $\mathcal{F} = \mathcal{G} = 0$ , we easily compute

$$u^* = b + a, \quad v^* = \frac{b}{(b + a)^2}$$

where  $b > 0$  and  $b + a > 0$ . For the linear stability of the non-diffusive Schnakenberg model, the homogeneous steady state conditions in (14) must be satisfied.

$$b - a < (b + a)^3, \quad (a + b)^2 > 0.$$

The Jacobian of the Schnakenberg kinetics is calculated as

$$\frac{\partial}{\partial u} \mathcal{F}(u, v) = 2uv - 1, \quad \frac{\partial}{\partial v} \mathcal{F}(u, v) = u^2, \quad \frac{\partial}{\partial u} \mathcal{G}(u, v) = -2uv, \quad \frac{\partial}{\partial v} \mathcal{G}(u, v) = -u^2.$$

The linearized system at steady state is defined as

$$\frac{d}{dt} \begin{pmatrix} u \\ v \end{pmatrix} = \gamma \begin{pmatrix} 2u^*v^* - 1 & u^{*2} \\ -2u^*v^* & -u^{*2} \end{pmatrix} \begin{pmatrix} u \\ v \end{pmatrix},$$

which results to eigenvalue problem

$$\mathcal{W}_t = \lambda \mathcal{W}, \quad \lambda = \gamma \mathbf{A}, \quad (16)$$

where

$$\mathbf{A} = \begin{pmatrix} a_{11} & a_{12} \\ a_{21} & a_{22} \end{pmatrix} = \begin{pmatrix} \frac{2b}{a+b} - 1 & (b + a)^2 \\ -\frac{2b}{a+b} & -(b + a)^2 \end{pmatrix} \begin{pmatrix} u \\ v \end{pmatrix},$$

with characteristic polynomial

$$\lambda^2 - (a_{11} + a_{22}) + (a_{11}a_{22} - a_{12}a_{21}).$$

We require  $Re(\lambda) < 0$ ,  $a_{11} + a_{22} < 0$  and  $(a_{11}a_{22} - a_{12}a_{21}) > 0$ , bear in mind that  $\mathcal{F}_v = a_{12} > 0$  and  $\mathcal{G}_u = a_{21} < 0$ .

To examine the diffusion-driven instability conditions for the Schnakenberg dynamics. First, we require to find the eigenvalue problem and evaluate its characteristic polynomial. Assume  $\lambda$  is dependent on the eigenvalue  $k^2$ ,

$$\mathcal{B} = \gamma\mathbf{A} - k^2\mathcal{D}$$

where  $\mathcal{D} = \begin{pmatrix} 1 & 0 \\ 0 & d \end{pmatrix}$  and  $k$  is wave number. Then, one can evaluate as

$$0 = (\mathcal{B} - \lambda\mathbf{I})\mathcal{W} \quad (17)$$

$$= \left[ \gamma \begin{pmatrix} a_{11} & a_{12} \\ a_{21} & a_{22} \end{pmatrix} - \begin{pmatrix} k^2 & 0 \\ 0 & dk^2 \end{pmatrix} - \begin{pmatrix} \lambda & 0 \\ 0 & \lambda \end{pmatrix} \right] \mathcal{W}. \quad (18)$$

Then,

$$\det(\mathcal{B} - \lambda\mathbf{I}) = \lambda^2 - \lambda[-k^2(1+d) + \gamma(a_{11} + a_{22})] + \phi(k^2)$$

where

$$\phi(k^2) = dk^4 - k^2(\gamma(a_{11}d + a_{22})) + \gamma^2(a_{11}a_{22} - a_{12}a_{21}). \quad (19)$$

It follows from the characteristic equation

$$\lambda^2 - \lambda\tau_{\mathcal{B}} + \nabla_{\mathcal{B}}, \quad \text{one obtains the roots } \lambda_{1,2} = \frac{\tau_{\mathcal{B}} \pm \sqrt{\tau_{\mathcal{B}}^2 - 4\nabla_{\mathcal{B}}}}{2}$$

with  $\tau_{\mathcal{B}} = (a_{11} + a_{22}) - k^2(1+d)$  and  $\nabla_{\mathcal{B}} = \phi(k^2)$ . It is obvious from a known result that in absence of diffusion, we stability provided  $Re(\lambda(0)) < 0$ , we have  $a_{11} + a_{22} < 0$ . Since  $k^2(1+d) > 0$ , then  $\tau_{\mathcal{B}} < 0$ . To guarantee the condition  $Re(\lambda(k^2)) > 0$ , we require  $\phi(k^2) < 0$ . Next, we need to know the value of  $\phi$  that will satisfy this outcome by calculating when  $\phi_{\min} < 0$ .

$$\frac{\partial\phi}{\partial k^2} = 2dk^2 - (a_{11}d + a_{22})\gamma,$$

so that  $k^2 = (a_{11}d + a_{22})/2d$  which on substituting into (19) yields

$$\phi_{\min} = \left( (a_{11}a_{22} - a_{12}a_{21}) - \frac{(a_{11}d + a_{22})^2}{4d}\gamma^2 \right) \Rightarrow (a_{11}a_{11} - a_{12}a_{21}) < \frac{(a_{11}d + a_{22})^2}{4d}. \quad (20)$$

It shows that at  $\phi_{\min} = 0$ , we have the bifurcation value of diffusion-driven instability. Following a similar process at the bifurcation point  $\phi$ , we can obtain a critical value for the diffusion coefficient denoted for brevity as  $d_c$ . Note,  $4d_c(a_{11}a_{22} - a_{12}a_{21}) = (d_c a_{11} + a_{22})^2$  and  $d_c^2 a_{11}^2 + 2(2a_{12}a_{21} - a_{11}a_{22})d_c + a_{22}^2 = 0$ . By requiring  $\phi(k^2) < 0$ , a necessary condition for instability is reached but not sufficient for diffusion-driven instability.

For  $d_c > 1$ , we can establish that  $d > d_c$  and give unstable modes that corresponds to  $k^2$  in the range

$$\gamma L_{\min}(a, b, d) < k^2 < \gamma L_{\max}(a, b, d), \quad (21)$$

where

$$L_{min} = \frac{[d(b-a) - (b+a)^3] - \{[d(b-a) - (b+a)^3]^2 - 4d(b+a)^4\}^{1/2}}{2d(b+a)}, \quad (22)$$

$$L_{max} = \frac{[d(b-a) - (b+a)^3] + \{[d(b-a) - (b+a)^3]^2 - 4d(b+a)^4\}^{1/2}}{2d(b+a)} \quad (23)$$

The points  $L_{min}$  and  $L_{max}$  is the range to find the wave numbers or eigenvalues that will present the solution of the reaction-diffusion system. Finally, this condition is found sufficient for large  $\gamma$ .

**Theorem 3.1.** *Consider the two-variable chemical species (11) with steady state  $(u^*, v^*)$ . Turing patterns are formed in (15) if the following conditions are satisfied:*

$$\mathcal{F}_u + \mathcal{G}_v < 0, \quad (24)$$

$$\mathcal{F}_u \mathcal{G}_v - \mathcal{F}_v \mathcal{G}_u > 0, \quad (25)$$

$$d\mathcal{F}_u + \mathcal{G}_v > 0, \quad (26)$$

$$(d\mathcal{F}_u + \mathcal{G}_v)^2 - 4d(\mathcal{F}_u \mathcal{G}_v - \mathcal{F}_v \mathcal{G}_u) > 0, \quad (27)$$

where all the derivatives are linearized at  $(u^*, v^*)$ . Depending on the key parameter  $\gamma$ , there exists a range of patterns if conditions (24-27) are satisfied.

*Proof* It follows directly from conditions (24) and (26) that  $d \neq 1$ , and derivatives  $\mathcal{F}_u, \mathcal{G}_v$  must have opposite signs which implies that  $b > a$  is required. In terms of reaction-diffusion, it indicates that the diffusion of the inhibitor is expected to diffuse faster than that of the activator of system (15).

Recall that the Jacobian of the dynamical system at  $(u^*, v^*)$  gives

$$\mathbf{A} = \begin{pmatrix} \frac{b-a}{a+b} & (b+a)^2 \\ -\frac{2b}{a+b} & -(b+a)^2 \end{pmatrix},$$

and by condition (24) of Theorem 3.1, we have

$$tr \mathbf{A} = \frac{b-a}{a+b} - (b+a)^2 < 0$$

therefore,  $0 < b-a < (b+a)^3$ .

By condition (25) of Theorem 3.1,

$$\begin{aligned} |\mathbf{A}| &= - \left[ \frac{b-a}{a+b} (b+a)^2 \right] - \left[ (b+a)^2 \left( -\frac{2b}{a+b} \right) \right] \\ &= b^2 + a^2 + 2ba \\ &= (b+a)^2 \\ &> 0. \end{aligned}$$

Similarly from condition (26) of Theorem 3.1, we have that

$$d\mathcal{F}_u + \mathcal{G}_v > 0,$$

which means that  $d(b - a) > (b + a)^3$ .

Finally, condition (27) of Theorem 3.1 says that

$$(d\mathcal{F}_u + \mathcal{G}_v)^2 - 4d(\mathcal{F}_u\mathcal{G}_v - \mathcal{F}_v\mathcal{G}_u) > 0,$$

it thus implies that  $[d(b - a) - (b + a)^3] > 4d(b + a)^4$ .

The four conditions in Theorem 3.1 are satisfied, a domain in the  $(a, b, d)$  parameter space is established, known as the pattern formation space or Turing space. Hence, there exist pattern formation for the Schnakenberg system. The proof is completed.  $\square$

Parabolic system (15) can be simplified further if rescaled. For instance, if new time variable  $\tilde{t} = \gamma \cdot t$  is introduced, and let  $\epsilon = 1/\gamma$ , it yields an equivalent parabolic system

$$\begin{aligned} u_t &= \epsilon \nabla u + \mathcal{F}(u, v) \quad \text{in } \Omega, \\ v_t &= d\epsilon \nabla v + \mathcal{G}(u, v) \quad \text{in } \Omega, \\ \nu \cdot \nabla u &= \nu \cdot \nabla v = 0 \quad \text{on } \partial\Omega, \end{aligned} \tag{28}$$

where  $\Omega = (0, H) \times (0, H) \subset \mathbf{R}^n$  and  $\nu$  is the unit normal on  $\partial\Omega$ . As seen above, we have studied (15) for large  $\gamma$ . In view of the rescaled parameter, we want to examine the behaviour of (28) for small values of  $\epsilon > 0$ . The following propositions are given in the spirit of [20] for the domain  $\Omega$  and nonlinearity of reaction kinetics  $\mathcal{F}$  and  $\mathcal{G}$ .

**Proposition 3.2. (Domain  $\Omega$ ).** *Assume that  $\Omega \subset \mathbf{R}^n$  is bounded domain with a Lipschitz continuous boundary  $\partial\Omega$ , for  $n \in \{1, 2, 3\}$ .*

**Proposition 3.3. (Smoothness of the nonlinearities of kinetics  $\mathcal{F}$  and  $\mathcal{G}$ ).** *Let  $\iota \in \mathbb{N}$  be arbitrary. (We choose  $\iota = 1$  when applying to reaction-diffusion system) Assume that  $\mathcal{F}, \mathcal{G} : \mathbf{R}^2 \rightarrow \mathbf{R}$  are  $C^{1+\iota}$ -are nonlinear functions, and there exist a point  $(u^*, v^*) \in \mathbf{R}^2$  with  $\mathcal{F}(u^*, v^*) = \mathcal{G}(u^*, v^*) = 0$ . We also propose further that if  $\iota \geq 2$ , all the partial derivatives of  $\mathcal{F}$  and  $\mathcal{G}$  of order  $2, 3, \dots, \iota$  at  $(u^*, v^*)$  vanish.*

Proposition 3.3 indicates that  $(u^*, v^*)$  is a steady state (equilibrium) solution of (28) for arbitrary  $\iota > 0$ .

**Proposition 3.4. (Turing instability).** *Let  $\mathcal{F}$  and  $\mathcal{G}$  remain as in proposition 3.3, for some  $d > 0$  we have conditions (24-27) of Theorem 3.1 as well as*

$$\mathcal{F}_u > 0, \tag{29}$$

$$(\mathcal{F}_u + \mathcal{G}_v)^2 - 4(\mathcal{F}_u\mathcal{G}_v - \mathcal{F}_v\mathcal{G}_u) > 0. \tag{30}$$

*The partial derivatives are evaluated at the point  $(u^*, v^*)$ . Due to conditions (24), (26) and (29), we must have  $d > 1$ .*

The inequalities in (24-27) of Theorem 3.1 are conditions responsible for the occurrence of a Turing instability. The inequalities (24) and (25) ensure the stability of the homogeneous steady state in the absence of diffusion, while (26) and (27) guarantee the instability of the homogeneous equilibrium state. Without loss of generality, condition (29) can be assumed: As a result of (24) and (26) the partial derivatives  $\mathcal{F}$  and  $\mathcal{G}$  are expected to have opposite signs, hence (29) is satisfied by rescaling system (28) and exchange both  $u$  and  $v$  in accordance with  $\mathcal{F}$  and  $\mathcal{G}$ . Lastly, inequality (30) shows that without diffusion the eigenvalues of the linearized system are real.

**Theorem 3.5. (Pattern formation)** [20, 21]. Assume that ecological system (28) satisfies Propositions (3.2-3.4). If we choose any constant  $\alpha$  with  $\dim \Omega/4 < \alpha < 1$ , and let  $0 < d_0 \ll 1$  be arbitrary, but fixed. Then there exists an  $\epsilon_0 > 0$ , such that for every  $0 < \epsilon \leq \epsilon_0$  there exists a finite dimensional subspace  $\mathcal{S}_\epsilon^+$  and radii  $0 < r_\epsilon < R_\epsilon$  such that the following is satisfied. In the limit  $\epsilon \rightarrow 0$ , we have

$$\dim \mathcal{S}_\epsilon^+ \sim \epsilon^{-\dim \Omega/2}, \quad r_\epsilon \sim \epsilon^{(2\alpha + \dim \Omega)/(2\iota)} \quad \text{and} \quad R_\epsilon \sim \epsilon^{-\dim \Omega/2}, \quad r_\epsilon \sim \epsilon^{(2\alpha + \dim \Omega)/(2\iota)}.$$

In addition, for some initial conditions  $(u_0, v_0) \in \mathbf{x}^\alpha$  satisfying

$$\|(u_0, v_0) - (u^*, v^*)\|_* < r_\epsilon,$$

the corresponding solution  $(u, v)$  of (28) exists a ball in a small neighbourhood of the homogeneous equilibrium  $(u^*, v^*)$  of radius  $R_\epsilon$ , and upon exiting the ball distance of  $(u, v)$  to the subspace  $\mathcal{S}_\epsilon^+$  is at most  $d_0 \cdot R_\epsilon$ .

**Theorem 3.6. (Linear behaviour).** Consider the reaction-diffusion Schnakenberg system (28), assume that Propositions (3.2-3.4) are satisfied, and let  $\rho > 0$  be arbitrarily small, but fixed. Let  $(u_0, v_0)$  be the initial condition close to the homogeneous equilibrium  $(u^*, v^*)$ , which is sufficiently close to the dominating subspace  $\mathcal{S}_\epsilon^+$ . In addition, we let  $(u, v)$  and  $(u_\alpha, v_\alpha)$  be the solutions to system (28) and its affine approximation at  $(u^*, v^*)$ , respectively, starting at  $(u_0, v_0)$ . Then the solution  $(u, v)$  remains close to  $(u_\alpha, v_\alpha)$  until the distance from  $(u, v)$  to the homogeneous equilibrium exceeds a certain threshold. Precisely, if

$$\|(u(t), v(t)) - (u^*, v^*)\|_* \leq C \cdot \epsilon^{-(\alpha - \dim \Omega/4) + \alpha/\iota + \rho} \cdot \|(u_0, v_0) - (u^*, v^*)\|_*^\rho$$

we have

$$\frac{\|(u(t), v(t)) - (u_\alpha(t), v_\alpha(t))\|_*}{\|(u_\alpha(t), v_\alpha(t)) - (u^*, v^*)\|_*} \leq C \cdot \epsilon^{\alpha - \dim \Omega/4}.$$

For details proof of Theorems 3.5 and 3.6, readers are referred to [20, 21].

## 3.2 Gray-Scott system

The second two-variable system of interest is the known Gray-Scott [22, 23, 24] autocatalytic model

$$\begin{aligned} u_t - D_u \nabla u &= \mathcal{F}(u, v) = -uv^2 + F(1 - u), \\ v_t - D_v \nabla v &= \mathcal{G}(u, v) = uv^2 - (F + k)v \end{aligned} \quad (31)$$

where  $u = u(\mathbf{X}, t)$  and  $v = v(\mathbf{X}, t)$ ,  $\mathbf{X} \in \mathbf{R}$  are the concentrations of two chemical species representing the inhibitor  $u$  and activator  $v$  respectively.  $F$  and  $k$  are the dimensionless control parameters denoting the flow rate and decay constant of the activator, while  $D_u, D_v$  are the diffusion coefficients.

Mathematical study of the Gray-Scott model has gone so wide over the last few decades, due to some delicate features that are not easy for numerical method to obtain, which are susceptible to small perturbations leading to instabilities. The model has provided an interesting test ground for theoreticians exploring the process of pattern formations such as spots and stripes [19, 25, 26], pulse splitting and the known auto-solitons as well as their

stability [27, 28, 29]. It should be noted that the model (31) also arises in biological contexts and rescale by different authors according to the biology/physics they wish to emphasize. Readers are referred to the classical book of Murray [19] for details.

As usual, in order to find the homogeneous equilibrium points of nonlinear system (31), we let  $\mathcal{F}(u, v) = 0$ ,  $\mathcal{G}(u, v) = 0$ , and after some algebraic manipulations we obtain  $v(v^2(F + k) - vF + F^2 + Fk) = 0$ , thus either  $v = 0$  with  $u = 1$  or  $v$  is determined from the root of the polynomial

$$v^2(F + k) - vF + F^2 + Fk. \quad (32)$$

That is

$$v = \frac{F \pm \sqrt{F^2 - 4(F + k)(F^2 + Fk)}}{2(F + k)}. \quad (33)$$

By using  $uv^2 - (F + k)v$ , we obtain  $u = (F + k)/v$ . To save time and space, we shall justify the linear analysis results with some basic theorems.

**Theorem 3.7.**  $\lim_{k \rightarrow 0}(u + v) = 1$ .

*Proof* We know that as  $k \rightarrow 0$ , also

$$v \rightarrow \frac{F \pm \sqrt{F^2 - 4(F + k)(F^2 + Fk)}}{2(F + k)} = \frac{1}{2} \pm \sqrt{1/4 - F}$$

known that  $u \rightarrow F/v$ . Thus

$$\begin{aligned} \lim_{k \rightarrow 0} u &= \frac{F}{1/2 \pm \sqrt{1/4 - F}} = \frac{F(1/2 \pm \sqrt{1/4 - F})}{1/4 - (1/4 - F)} = 1 - (1/2 \pm \sqrt{1/4 - F}) \\ &= 1 - \lim_{k \rightarrow 0} v, \end{aligned}$$

which means that  $\lim_{k \rightarrow 0}(u + v) = 1$ . □

**Definition 3.8.** *In absence of diffusion, an equilibrium point of the Gray-Scott system (31) is said to be stable if small perturbations from the equilibrium have no effect on the solution at steady state. That is, when a small perturbation from equilibrium settles back to the equilibrium point. In mathematics, it is referred to as a constant solution to a differential equation.*

The matrix stability for the Gray-Scott system (31) is given by

$$\mathbf{J}_{(u^*, v^*)} = \begin{pmatrix} -v^2 - F & -2uv \\ v^2 & uv - (F + k) \end{pmatrix}, \quad (34)$$

we can see that the linear stability of (31) depends on the equilibrium points and ultimately on parameter values  $F$  and  $k$ .

**Theorem 3.9.** *The homogeneous equilibrium point  $(u^*, v^*) = (1, 0)$  is always stable for (31).*

*Proof* At point  $(u^*, v^*)$ ,

$$\mathbf{J}_{(u^*, v^*)} = \begin{pmatrix} -F & 0 \\ 0 & -(F+k) \end{pmatrix}. \quad (35)$$

Equation (35) has eigenvalues  $-F$  and  $-(F+k)$ . In biological contexts, both the feed rate  $F$  and the constant rate  $k$  must be positive numbers, the eigenvalue of matrix (35) must always be negative for any meaningful choice of parameters  $F$  and  $k$ .  $\square$

**Theorem 3.10.** *The nontrivial equilibrium point*

$$(\hat{u}, \hat{v}) = \left( \frac{F+k}{v}, \frac{F + \sqrt{F^2 - 4(F+k)(F^2 + Fk)}}{2(F+k)} \right)$$

*is always unstable for all possible values of  $F$  and  $k$ .*

*Proof* At point  $(\hat{u}, \hat{v})$ ,

$$\mathbf{J}_{(\hat{u}, \hat{v})} = \begin{pmatrix} -v^2 - F & -2(F+k) \\ v^2 & F+k \end{pmatrix}. \quad (36)$$

We calculate the determinant of this matrix as

$$\det \mathbf{J}_{(\hat{u}, \hat{v})} = (F+k)(v^2 - F).$$

We aim to show that  $(v^2 - F)$  is always negative for all possible values of parameters  $F$  and  $k$ . Known that the equilibrium point's  $v$  is given by

$$\hat{v} = \frac{F - \sqrt{F^2 - 4F(F + Fk)^2}}{2(F+k)}.$$

We let the discriminant be between 0 and 1; that is  $0 \leq F^2 - 4F(F + Fk)^2 \leq 1$ . It follows that

$$F^2 - 4(F + Fk)^2 \leq F^2 - 4F(F + Fk)^2 \leq \sqrt{F^2 - 4F(F + Fk)^2}.$$

In the spirit of [19, 25], the inequality on the left is satisfied because  $F \leq 1/4 < 1$ , so also the inequality sign on the right is true since the term inside the discriminant is less than one. We can rearrange the inequality to get  $v$  as

$$F^2 - \sqrt{F^2 - 4F(F + Fk)^2} \leq 4(F+k)^2, \quad v = \frac{F^2 - \sqrt{F^2 - 4F(F + Fk)^2}}{2(F+k)} \leq 2(F+k).$$

The last expression is manipulated further into a more convenient form

$$\frac{vF}{F+k} \leq 2F, \quad \frac{vF - F(F+k)}{F+k} - F \leq 0. \quad (37)$$

We can obtain expression  $v^2$  in terms of  $v$  from (32). Which implies

$$v^2 = \frac{vF - F(F+k)}{F+k}, \quad (38)$$

now using equations (37) and (38) we can easily verify that

$$v^2 - F = \frac{vF - F(F+k)}{F+k} - F \leq 0$$

which indicate that  $\det \mathbf{J}_{(\hat{u}, \hat{v})}$  is negative. In conclusion, both eigenvalues are real with one eigenvalue positive, and the other negative. so, the equilibrium point  $(\hat{u}, \hat{v})$  is always unstable for all  $F$  and  $k$  parameter values.  $\square$

In the work of Murray [19] and other researchers [18, 30, 31, 32], studies have shown that diffusion contributes in no small measure to stability in a system, it increases the concentrations of lower regions, and decreases concentrations of the higher regions. As a result, pattern formation in the form of nonhomogeneous steady-state and periodic solutions is eminent.

**Theorem 3.11.** *For diffusion-driven instability to occur in two variable reaction-diffusion system, the diffusion coefficients must not be equal. For a homogeneous equilibrium state  $(\bar{u}, \bar{v})$  of the non-diffusive system*

$$u_t = \mathcal{F}(u, v), \quad v_t = \mathcal{G}(u, v) \quad (39)$$

to be linearly stable, and linearly unstable for the diffusive system

$$u_t = D_u \nabla u + \mathcal{F}(u, v), \quad v_t = D_v \nabla v + \mathcal{G}(u, v), \quad (40)$$

$D_u \neq D_v$ .

*Proof* For homogeneous equilibrium point  $(\bar{u}, \bar{v})$  to be linearly stable for (39), the conditions  $\text{tr} \mathbf{J} = \mathcal{F}_u + \mathcal{G}_v < 0$  and  $\det \mathbf{J} = \mathcal{F}_u \mathcal{G}_v - \mathcal{F}_v \mathcal{G}_u > 0$  must be satisfied. If we let  $D_u = D_v = D_{uv}$ , our determinant becomes

$$\delta_{ij}^2 D_{uv}^2 + \delta_{ij} D_{uv} (\mathcal{F}_u + \mathcal{G}_v) + (\mathcal{F}_u \mathcal{G}_v - \mathcal{F}_v \mathcal{G}_u), \quad (41)$$

$\delta_{ij}$  is a negative scalar depending on the basis function used. The first term in expression (41) is always positive. Since  $\delta_{ij}$  is negative, the second term is also positive, the diffusion coefficient  $D_{uv} > 0$ , and  $(\mathcal{F}_u + \mathcal{G}_v) < 0$ . More-so, the last term  $(\mathcal{F}_u \mathcal{G}_v - \mathcal{F}_v \mathcal{G}_u) > 0$ , and condition

$$\delta_{ij}^2 (D_u D_v) + \delta_{ij} (\mathcal{G}_v D_u + \mathcal{F}_u D_v) + (\mathcal{F}_u \mathcal{G}_v - \mathcal{F}_v \mathcal{G}_u) > 0 \quad (42)$$

hold. With equal diffusivity, we have the trace  $\mathcal{F}_u + \mathcal{G}_v + 2\delta_{ij} D_{uv} < 0$ . Thus  $(\bar{u}, \bar{v})$  always satisfy the sufficient conditions for diffusive system (40) to be stable. There will be no diffusion-driven instability.  $\square$

**Theorem 3.12.** *The homogeneous equilibrium solution to the Gray-Scott reaction-diffusion system (31) at point  $(u^*, v^*) = (1, 0)$  is linearly stable for all values of  $F$ ,  $k$ ,  $D_u$  and  $D_v$ .*

*Proof* Known that the point  $(u^*, v^*) = (1, 0)$  is the homogeneous solution for system (31). The matrix  $J$  for the Gray-Scott reaction-diffusion system (31) is

$$\mathbf{J} = \begin{pmatrix} -v^2 - F & -2uv \\ v^2 & 2uv - (F+k) \end{pmatrix}, \quad (43)$$

we define matrix  $A_{ij}$  by

$$\mathbf{A}_{ij} = \begin{pmatrix} -v^2 - F + \delta_{ij}D_u & -2uv \\ v^2 & 2uv - (F + k) + \delta_{ij}D_v \end{pmatrix}, \quad (44)$$

and

$$\mathcal{F}_u + \mathcal{G}_v + \delta_{ij}(D_u + D_v) = \text{tr}(A_{ij}) < 0 \quad (45)$$

the left hand side of (45) yields  $\delta_{ij}^2 D_u D_v - \delta_{ij}(F D_v + (F + k) D_u) + F(F + k)$ . Since  $\delta_{ij} < 0$  and the diffusion parameters are positive and condition (42) always satisfied. For point  $(u^*, v^*)$ , the left hand side of condition (45) yields

$$\delta_{ij}(D_u + D_v) - 2F - k. \quad (46)$$

Since expression (46) is negative, the condition (45) is satisfied. So, both conditions (42) and (45) are satisfied, the equilibrium point  $(u^*, v^*)$  is stable for all reaction-diffusion parameters  $F, k, D_u$  and  $D_v$ .  $\square$

In what follows, we now work on the applicability and suitability of the Fourier transform for solving space fractional reaction-diffusion models.

## 4 Fractional Fourier spatial discretisation

The powers  $(-\Delta)^{\alpha/2}$  of the positive Laplace operator  $(-\Delta)$ , in a bounded domain  $\Omega$  with zero Dirichlet or Neumann boundary data, are defined through the spectral decomposition using the powers of the eigenvalues of the original operator. Let  $(\varphi_j, \lambda_j)$  be the eigenfunctions and eigenvectors of  $(-\Delta)$  in  $\Omega$  with zero Dirichlet or Neumann boundary data. Then  $(\varphi_j, \lambda_j^{\alpha/2})$  are the eigenfunctions and eigenvectors  $(-\Delta)^{\alpha/2}$ , also with Dirichlet or Neumann boundary conditions. In fact, the fractional Laplacian  $(-\Delta)^{\alpha/2}$  is well defined in the space of functions

$$H_0^{\alpha/2}(\Omega) = \left\{ u = \sum_{j=0}^{\infty} a_j \lambda_j^{\alpha/2} \in L^2(\Omega) : \|u\|_{H_0^{\alpha/2}(\Omega)} = \left( \sum_{j=0}^{\infty} a_j^2 \lambda_j^{\alpha/2} \right)^{1/2} < \infty \right\} \quad (47)$$

where

$$\|u\|_{H_0^{\alpha/2}(\Omega)} = \|(-\Delta)^{\alpha/4} u\|_{L^2(\Omega)}. \quad (48)$$

Therefore for any  $u \in H_0^{\alpha/2}$ , the Laplacian  $(-\Delta)^{\alpha/2}$  is defined by

$$(-\Delta)^{\alpha/2} u = \sum_{i=0}^{\infty} a_i \lambda_i^{\alpha/2} \varphi_i, \quad (49)$$

where  $\varphi_j$  and  $\lambda_j$  will depend on the specified boundary conditions.

For homogeneous Dirichlet boundary condition we have

$$(\varphi_j, \lambda_j) = \left( \left[ \frac{(j+1)\pi}{b-a} \right]^2, \sqrt{\frac{2}{b-a}} \sin \left[ \frac{(x-a)\pi(j+1)}{b-a} \right] \right), \quad (50)$$

whereas for homogeneous Neumann boundary condition we obtain

$$(\varphi_j, \lambda_j) = \left( \left[ \frac{\pi j}{b-a} \right]^2, \sqrt{\frac{2}{b-a}} \sin \left[ \frac{(x-a)\pi j}{b-a} \right] \right). \quad (51)$$

This approach gives a full diagonal representation of the fractional operator and achieves spectral convergence regardless of the fractional power in the problem. Meanwhile, the application to high spatial dimensions is the same as the one-dimensional problem. However, the nonlinear term is evaluated in physical space and then transformed to Fourier space. This can cause problems with aliasing, and one has to be careful to filter high frequencies appropriately.

To illustrate this approach, we apply the fast Fourier transform to the fractional reaction-diffusion equation of the general form [33]

$$\begin{cases} u_t = K_u(\Delta^{\alpha/2})u + f(u, v), \\ v_t = K_v(\Delta^{\alpha/2})v + g(u, v), \end{cases} \quad (52)$$

to obtain the two dimensional representation of (52) in Fourier space

$$\begin{aligned} U_t(\chi_x, \chi_y, t) &= -K_u((\chi_x^2)^{\alpha/2} + (\chi_y^2)^{\alpha/2})U(\chi_x, \chi_y, t) + \mathcal{F}[f(u(x, y, t), v(x, y, t))], \\ V_t(\chi_x, \chi_y, t) &= -K_v((\chi_x^2)^{\alpha/2} + (\chi_y^2)^{\alpha/2})V(\chi_x, \chi_y, t) + \mathcal{F}[g(u(x, y, t), v(x, y, t))], \end{aligned}$$

where  $U$  and  $V$  are the double Fourier transforms of the chemical concentrations  $u(x, y, t)$  and  $v(x, y, t)$ , respectively. In other words,

$$\begin{aligned} \mathcal{F}[u(x, y, t)] &= U(\chi_x, \chi_y, t) = \int_0^\infty \int_0^\infty u(x, y, t) e^{-i(\chi_x x + \chi_y y)} dx dy, \\ \mathcal{F}[v(x, y, t)] &= V(\chi_x, \chi_y, t) = \int_0^\infty \int_0^\infty v(x, y, t) e^{-i(\chi_x x + \chi_y y)} dx dy, \\ \mathcal{F}[w(x, y, t)] &= W(\chi_x, \chi_y, t) = \int_0^\infty \int_0^\infty w(x, y, t) e^{-i(\chi_x x + \chi_y y)} dx dy. \end{aligned}$$

To explicitly remove the adherent stiffness in the second partial derivatives using integrating factors, we let  $\Omega^{\alpha/2} = ((\chi_x^2)^{\alpha/2} + (\chi_y^2)^{\alpha/2})$ , and set

$$U = e^{-K_u \Omega^{\alpha/2} t} \bar{U}, \quad V = e^{-K_v \Omega^{\alpha/2} t} \bar{V},$$

so that now we have

$$\begin{aligned} \partial_t \bar{U} &= e^{K_u \Omega^{\alpha/2} t} \mathcal{F}[f(u, v, w)], \\ \partial_t \bar{V} &= e^{K_v \Omega^{\alpha/2} t} \mathcal{F}[g(u, v, w)], \end{aligned} \quad (53)$$

Next, we need to discretize the square domain by considering the equispaced points  $N_x$  and  $N_y$  in the spatial directions of  $x$  and  $y$ . We employ the discrete fast Fourier transform (DFFT) [33, 34] to transform (53) to a system of ordinary differential equations (ODEs)

$$\begin{aligned} \partial_t \bar{U}_{i,j} &= e^{K_u \Omega_{i,j}^{\alpha/2} t} \mathcal{F}[f(u_{i,j}, v_{i,j}, w_{i,j})], \\ \partial_t \bar{V}_{i,j} &= e^{K_v \Omega_{i,j}^{\alpha/2} t} \mathcal{F}[g(u_{i,j}, v_{i,j}, w_{i,j})], \end{aligned} \quad (54)$$

where  $u_{i,j} = u(x_i, y_j)$ ,  $v_{i,j} = v(x_i, y_j)$  and  $\Omega_{i,j}^{\alpha/2} = (\chi_x^2(i))^{\alpha/2} + (\chi_y^2(j))^{\alpha/2}$ . Boundary conditions are now set at extremities of the domain. At this point, the system has been converted to ODEs, the stiffness property has equally been removed. It should be noted that any explicit higher-order time stepping methods can be used. However, we employ a fourth order exponential time differencing Runge-Kutta (ETD4RK) scheme which was proposed by Cox-Matthews [35]. We advance in time with the improved ETD4RK scheme [33, 36, 37, 38]

$$\begin{aligned}\mathcal{U}_{n+1} &= e^{\mathbf{L}h}\mathcal{U}_n + h[4\varphi_3(\mathbf{L}h) - 3\varphi_2(\mathbf{L}h) + \varphi_1(\mathbf{L}h)]\mathbf{F}(u_n, v_n, t_n) \\ &\quad + 2h[\varphi_2(\mathbf{L}h) - 2\varphi_3(\mathbf{L}h)]\mathbf{F}(\mu_2, t_n + h/2) \\ &\quad + 2h[\varphi_2(\mathbf{L}h) - 2\varphi_3(\mathbf{L}h)]\mathbf{F}(\mu_3, t_n + h/2) \\ &\quad + h[\varphi_3(\mathbf{L}h) - 2\varphi_2(\mathbf{L}h)]\mathbf{F}(\mu_4, t_n + h),\end{aligned}\tag{55}$$

with the stages  $\mu_i$  given as

$$\begin{aligned}\mu_2 &= e^{\mathbf{L}h/2}\mathcal{U}_n + (\mathbf{L}h/2)\varphi_1(\mathbf{L}h/2)\mathbf{F}(u_n, v_n, t_n) \\ \mu_3 &= e^{\mathbf{L}h/2}\mathcal{U}_n + (\mathbf{L}h/2)[\varphi_1(\mathbf{L}h/2) - 2\varphi_2(\mathbf{L}h/2)]\mathbf{F}(u_n, v_n, t_n) + h\varphi_2(\mathbf{L}h/2)\mathbf{F}(\mu_2, t_n + h/2) \\ \mu_4 &= e^{\mathbf{L}h}\mathcal{U}_n + h[(\varphi_1(\mathbf{L}h) - 2\varphi_2(\mathbf{L}h)]\mathbf{F}(u_n, v_n, t_n) + 2h\varphi_2(\mathbf{L}h)\mathbf{F}(\mu_3, t_n + h),\end{aligned}$$

with functions  $\varphi_{1,2,3}$  defined as

$$\varphi_1(z) = \frac{e^z - 1}{z}, \quad \varphi_2 = \frac{e^z - 1 - z}{z^2}, \quad \varphi_3 = \frac{e^z - 1 - z - z^2/2}{z^3}$$

which precisely coincide with the terms in the Lie group methods by Munthe-Kaas [39]. For details derivation and stability of the ETD4RK method, see [33, 36, 37].

## 5 Numerical experiments

Here, we are concerned mainly with the numerical simulations of two coupled reaction-diffusion equations systems discussed in Section 3, using the fractional exponential integrator scheme as introduced in Section 4. We choose to experiment our numerical method with the two nontrivial examples of space fractional reaction-diffusion equations in the last section. We realized that simulations in one dimension are easily undertaken [26, 40, 41], hence, we consider higher dimensional examples that are still of current and recurring interest with some feasible initial conditions that are capable of addressing the points and queries that may arise. Also in our numerical simulations, to ensure that we generate Turing patterns, two notable boundary conditions are chosen in the required spatial domain. All simulations run for  $N = 200$ , and are carried out in MATLAB.

### 5.1 Numerical convergence

In this section, we experiment the diffusive system (52) numerically by using the numerical method discussed in Section 4. The solutions are obtained using the initial data is biologically

meaningful. We demonstrate the efficiency and accuracy of the present method by reporting the relative  $\ell_\infty$ -norm error

$$\ell_\infty(N) = \frac{\|u - \tilde{u}\|_\infty}{\|u\|_\infty} = \max_{1 \leq j \leq N} \frac{|u_j - \tilde{u}_j|}{|u_j|}, \quad (56)$$

where  $u$  and  $\tilde{u}$  represent the exact and approximate solutions, respectively, and  $N$  the number of computational grids.

Reliability and efficiency of fractional Fourier transform method is justified in Figure 1 by reporting the relative errors as a function of number the number of grid points  $N$ . Let us consider for simplicity the one-dimensional space fractional heat equation in the absence of source term. This is obtained by considering  $f(U, t) = 0$ , from Equation (52). The fractional heat equation is subjected to the standard homogeneous Neumann boundary condition, the initial conditions are chosen to be

$$u(x, 0) = 100 \exp(-100x^2), \quad (57)$$

where  $x \in [-L, L]$ . Figure 1 shows numerical solutions of the heat equation together with the convergence of the fractional Fourier transform with different values of  $\alpha$  at final time  $T_f = 1$ . Since the solution of the fractional heat equation is exact in time, all of the error in scheme is associated with the spatial discretisation. Reference solutions were calculated by evaluating the fractional heat equation with  $2^{12}$  Fourier modes. Clearly, the fractional Fourier approach is able to achieve spectral convergence up to machine precision regardless of  $\alpha$ .

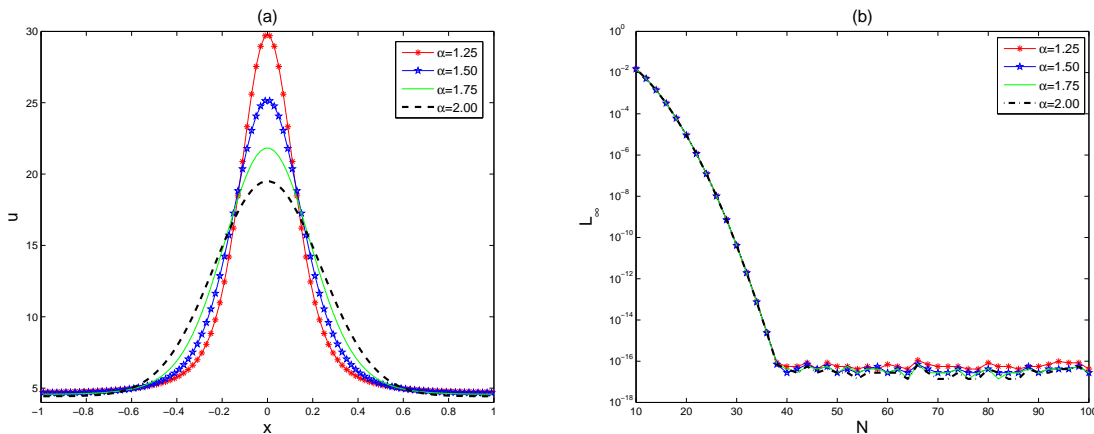


Figure 1: (a) Solution of the fractional heat equation and (b) convergence of the fractional Fourier method. The parameters are  $K_\alpha = 1$ ,  $L = 1$  and  $T_f = 0.1$ .

## 5.2 Two dimensional results for the Schnakenberg system

We proceed our numerical simulations in 2D with the evolution of fractional reaction-diffusion Schnakenberg (15). Based on our mathematical formulations and inline with (1), we need to transform the classical coupled reaction-diffusion Schnakenberg system (15) to a space

fractional reaction-diffusion type:

$$\begin{aligned}\frac{\partial u}{\partial t} &= \nabla^\alpha u + \gamma (a - u + u^2 v), \\ \frac{\partial v}{\partial t} &= d \nabla^\alpha v + \gamma (a - u + u^2 v).\end{aligned}\quad (58)$$

Equation (58) at  $\alpha = 1$  corresponds to standard reaction-diffusion system described by equation (15). At  $\alpha < 1$ , correspond to anomalous sub-diffusion and at  $\alpha > 1$ , describe anomalous super-diffusion. We consider (58) on a fixed square domain  $[0, 200] \times [0, 200]$  with no flux boundary conditions, and  $u, v \in \mathbf{R}^2$ . We let  $x, y \in \mathbf{R}^2$ ,  $\nabla = (\partial^2/\partial x^2 + \partial^2/\partial y^2)$  be the usual Laplacian operator of fractional order  $\alpha$  associated with the linear terms of  $u$  and  $v$  in two-dimensional space.

The initial condition

$$\begin{aligned}u(x, y, 0) &= u^* - \exp\left(-10\left(x - \frac{p}{2}\right)^2 + \left(y - \frac{p}{2}\right)^2\right) \\ v(x, y, 0) &= \exp\left(-10\left(x - \frac{p}{2}\right)^2 + v^*\left(y - \frac{p}{2}\right)^2\right)\end{aligned}\quad (59)$$

is chosen specifically so as to induce a nontrivial spatiotemporal dynamics. In the experiments, different types of dynamics are observed and we have realized that the distributions of  $u$  and  $v$  are always of the same pattern. Hence, we restrict our pattern formation analysis to only one distribution (for the Schnakenberg example, we show the distribution of  $v$ ).

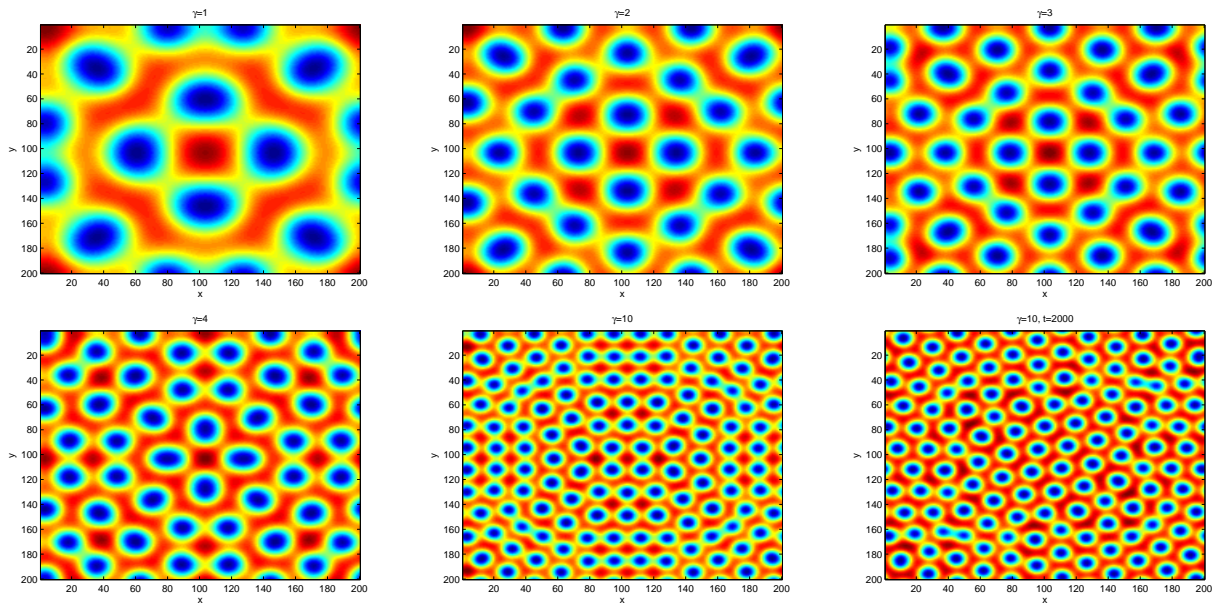


Figure 2: The snapshots of contour pictures for the time evolution of substrate  $v$  for the fractional reaction-diffusion Schnakenberg system (58) at different instants of  $\gamma$ . The simulation depicts the distribution of the species is the formation of Turing spot patterns. The parameters are taken as:  $\alpha = 1.8, a = 0.1, b = 0.9, d = 15, p = 1, u^* = 1, v^* = 2$  at final time  $t = 1000$ .

In Figure 2, we show the results of Turing stability analysis as discussed in Section 4 above for the super-diffusive case when  $\alpha = 1.8$ . These results confirm the presence of linear

instability for the parameter  $a < 1$ . That is, a Turing bifurcation occurs at the neighborhood of  $a = 1$ . The homogeneous steady state of Schnakenberg system (58) for  $a < 1$  is linearly unstable which guarantee pattern formation. A chain cluster of Turing spotted patterns initially evolve with  $\gamma = 1, 2, 3, 4, 10$ , but as simulation time is increased to 2000 for  $\gamma = 10$  we obtained a pure Turing spot patterns.

Based on our observation in Figure 2 which reflects the impact of increasing simulation time. As a result, we experiment at different instants of final time in Figure 3. Other parameters are fixed as in the figure caption.

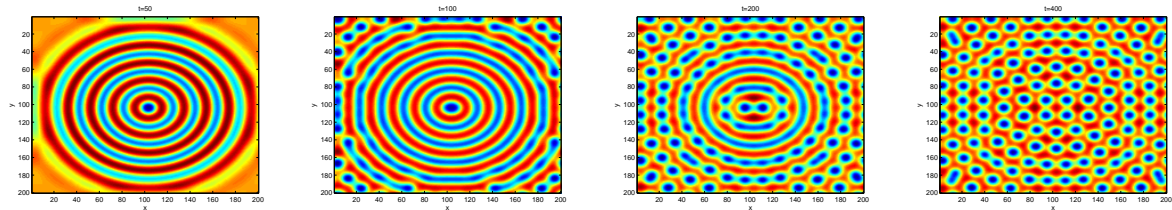


Figure 3: Snapshots of the evolution of substrate  $v$  for the system (58) at different instants of final time  $t$ , panels 1 to 4 correspond to doubling time  $t = 50, 100, 200, 400$  respectively. Parameter values are:  $\gamma = 10; a = 0.1, b = 0.9, d = 12, p = 1, (u^*, v^*) = (1, 2), \alpha = 1.5$ .

It should be noted that, it is very interesting to observe the dynamics of system (58) at different instants of time. The smooth and stable circular structures emerged at  $t = 50$ . As simulation time is doubled, that is at  $t = 100, 200, 400$ , the spiral structures are disintegrated from the boundary to the center of the domain to form Turing spot patterns. Other Turing patterns are possible to observe depending on the choice and variability of the parameters. In our last experiment for 2D system (58), we observe the effect of fractional power  $\alpha$  at different instants of 0.5, 1 and 1.5 which corresponds to the sub-diffusive, diffusive and super-diffusive results as shown in Figure 4.

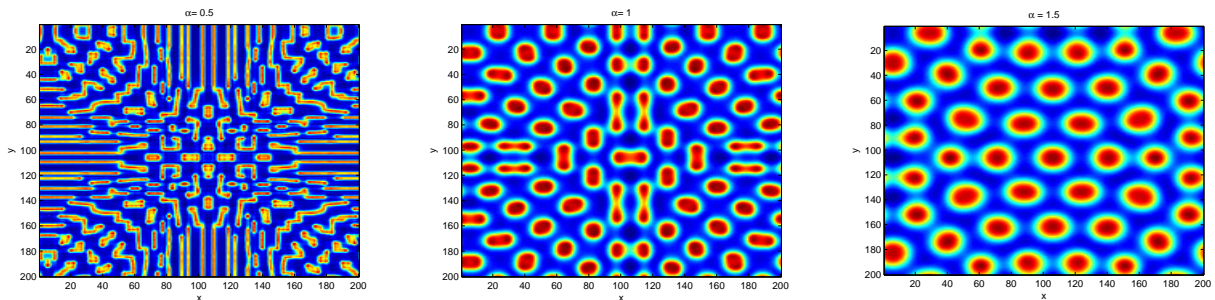


Figure 4: Numerical 2D solutions of the Fractional reaction-diffusion system (58) obtained at different instants of fractional power  $\alpha$ . Plot (a) corresponds to the sub-diffusive result at  $\alpha = 0.5$ , (b) is the standard diffusive result at  $\alpha = 1$ , and (c) the super-diffusive result at  $\alpha = 1.5$ . Other parameters are:  $d = 12, a = 0.1, b = 0.9, p = 1, \gamma = 10$ , on a fixed domain  $L = \pm 10$  at final time  $t = 1000$  with initial conditions (59).

### 5.3 Two dimensional results for the Gray-Scott system

For the example here, we first make substitutions  $A = F$  and  $B = F + 1$  in (31) [40] to obtain a coupled fractional-in-space partial differential equations

$$\frac{\partial u}{\partial t} = D_u \nabla^\alpha u - uv^2 + A(1 - u) \quad \frac{\partial v}{\partial t} = D_v \nabla^\alpha v + uv^2 - Bv, \quad (60)$$

where  $u = u(x, y, t)$  and  $v = v(x, y, t)$  remains the concentrations of chemical species  $u$  called the inhibitor, and  $v$  known as the activator respectively,  $\alpha$  as the fractional order for the diffusive terms. The parameter  $A > 0$  stands for the rate at which the inhibitor  $u$  is fed from the reservoir into a reactor, and  $B > 0$  is the overall rate of decay of  $v$  due to draining.  $\nabla$  is Laplacian operator of order  $\alpha$  with respect to positions  $x, y \in \mathbf{R}^2$  at time  $t$ .  $D_u$  and  $D_v$  are the diffusivities coefficients that denote the rate at which the two chemical species diffuse [40, 42]. We first experiment on a growing domain size  $[-L, L]$  subject to Neumann boundary conditions, and initial conditions taken as:

$$u(x, y, 0) = 1 - u^* \exp(-0.05(x^2 + y^2)), \quad v(x, y, 0) = v^* \exp(-0.05(x^2 + y^2)) \quad (61)$$

where  $(u^*, v^*)$  are fixed as  $(1/2, 1, 4)$ . In Figure 5, formation of Turing spots dynamic is

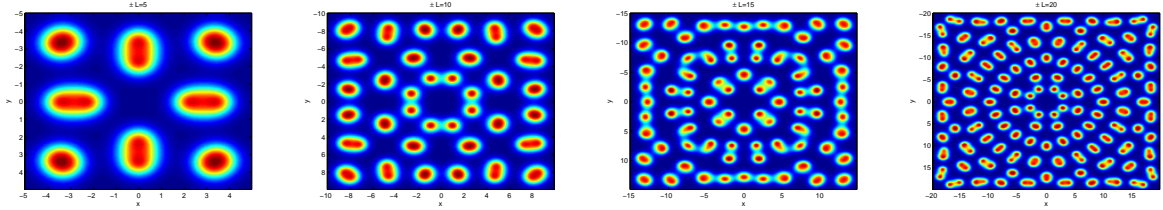


Figure 5: Snapshots of the evolution of substrate  $v$  for the Gray-Scott system (60) on a growing domain of size  $\pm L$  at final time  $t = 1000$  with initial conditions (61). Other parameters are:  $\alpha = 1.5$ ,  $A = g\epsilon$ ,  $B = 0.4\epsilon$ ,  $g = 9$ ,  $\epsilon = 0.005$ ,  $D_u = 2E - 5$  and  $D_v = 2D_u$ .

observed for the Gray-Scott equation (60) on a growing domain of size  $\pm L$ . Owing to the fact that both species have similar distributions in space, we also restrict our analysis to that of activator  $v$ . Further, we examine the 2D pattern formation in (60) by keeping the domain size of  $\pm L = 10$  and vary  $g = 2, 5, 7, 11$  as in Figure 6. The spots pattern comes in different shapes.

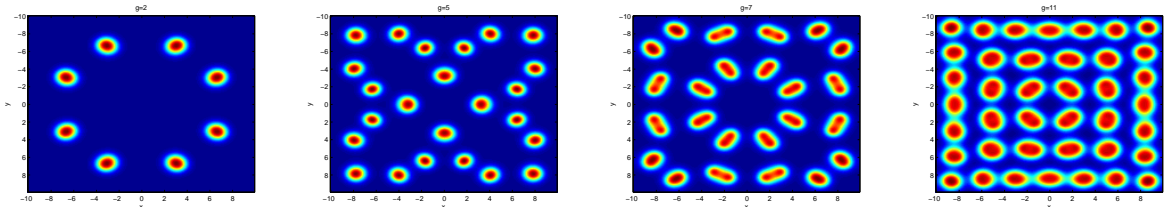


Figure 6: Snapshots of the evolution of substrate  $v$  for the Gray-Scott system (60) on a fixed domain  $\pm L = 10$  at final time  $t = 1000$  with initial conditions (61), at different instants of  $A = g\epsilon$ , for  $g = 2, 5, 7$  and  $11$ . Other parameters are:  $\alpha = 1.5$ ,  $B = 0.4\epsilon$ ,  $\epsilon = 0.005$ ,  $D_u = 2E - 5$  and  $D_v = 2D_u$ .

It should be noted that no pattern was obtained for fractional power  $\alpha$  in the interval  $0 < \alpha \leq 1$  which corresponds to sub-diffusive and classical diffusive regions respectively. Hence, we investigate the super-diffusive model at instances of  $\alpha = 1.5, 1.7, 1.9$  as shown in Figure 7.

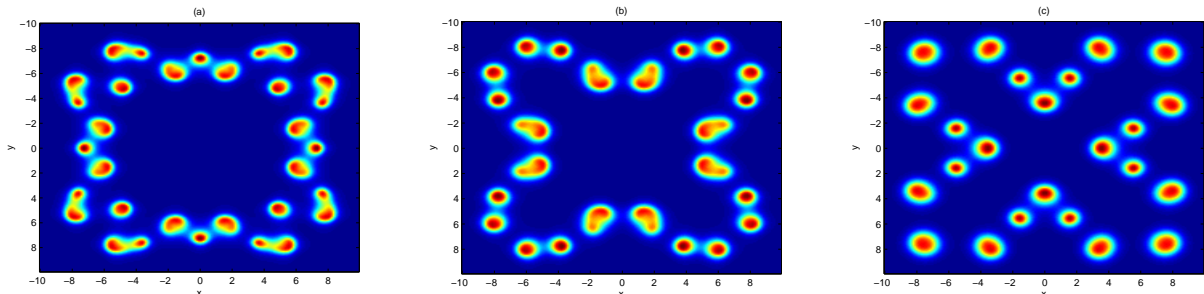


Figure 7: Super-diffusive 2D solutions of the Fractional reaction-diffusion system (60) obtained at different instants of fractional power  $\alpha$ . Plot (a) corresponds to result at  $\alpha = 1.5$ , (b) is obtained at  $\alpha = 1.7$ , and (c) at  $\alpha = 1.9$ . Other parameters are:  $A = 0.0250$ ,  $B = 0.0684$ ,  $D_u = 2E - 5$  and  $D_v = 2D_u$  at final time  $t = 2000$  with initial conditions (61).

## 5.4 Three dimensional experiments

In this section, we want to explore the dynamic richness of the fractional reaction-diffusion equations, starting with the Schnakenberg system (58) in three dimensions (3D). We let  $\nabla = (\partial^2/\partial x^2 + \partial^2/\partial y^2 + \partial^2/\partial z^2)$ , for  $u = (x, y, z, t), v = (x, y, z, t)$  subject to the initial functions

$$\begin{aligned} u(x, y, z, 0) &= 1 - \exp(-10((x - p/2)^2 + (y - p/2)^2 + (z - p/2)^2)), \\ v(x, y, z, 0) &= \exp(-10((x - p/2)^2 + 2(y - p/2)^2 + (z - p/2)^2)). \end{aligned} \quad (62)$$

Numerical simulation of fractional Schnakenberg model in three spatial dimensions provides amazing scenario for the emergence of more exotic and chaotic patterns in the parameter regime where pattern formation in form of wavefront is partially driven by  $\alpha$ .

It was observed in the experiment that both species have similar distribution. Hence, we also restrict our analysis of pattern formation to only the distribution of  $v$  species. In Figure 8, we observed three different dynamics as a result of varying effects of fractional order  $\alpha$  which classify the distribution into sub-diffusive, diffusive and super-diffusive cases. In Figure 9, we verify the effects of fractional power  $\alpha$  on sub-diffusive, diffusive and super-diffusive fractional reaction-diffusion form of (58) at different instants of domain size  $[-L, L]$ ,  $L = 5, 10, 20$ . The upper-row corresponds to the sub-diffusive results for  $\alpha = 0.5$ , the middle-row indicates patterns obtained for the standard diffusive model at  $\alpha = 1$ , and the lower-row for the super-diffusive model at  $\alpha = 1.5$ . As can be clearly appreciated in Figure 9, the chaotic structures gradually transformed into a smooth growing lobe in the super-diffusion case.

In a similar fashion, we experiment the fractional reaction-diffusion model (60) in 3D

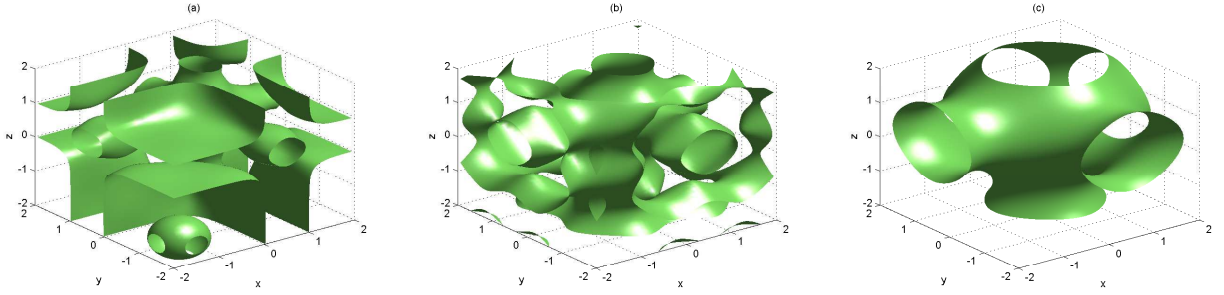


Figure 8: Snapshots of the evolution of substrate  $v$  for the Fractional reaction-diffusion system (58) in 3D at different instants of fractional power  $\alpha$ . Plot (a) corresponds to the sub-diffusive result at  $\alpha = 0.5$ , (b) is the standard diffusive form at  $\alpha = 1$ , and the super-diffusive result at  $\alpha = 1.5$  as in panel (c). Other parameters are:  $d = 12$ ,  $a = 0.1$ ,  $b = 0.9$ ,  $p = 1$ ,  $\gamma = 10$ , on a fixed domain  $L = \pm 2$  at final time  $t = 5$  with initial conditions (62).

with initial functions

$$\begin{aligned} u(x, y, z, 0) &= 1 - 0.5 \exp(-50((x - p/2)^2 + (y - p/2)^2 + (z - p/2)^2)), \\ v(x, y, z, 0) &= 0.25 \exp(-50((x - p/2)^2 + 2(y - p/2)^2 + (z - p/2)^2)). \end{aligned} \quad (63)$$

In the simulations, some chaotic dynamics are observed at different instants of fractional order parameter  $\alpha$  subject to the Neumann boundary conditions in  $[0, L]$ , for  $L = 5, 10$  and  $20$ . In the first row of Figure 10, we simulate for sub-diffusive, diffusive and super-diffusive types of (60) at instants of  $\alpha = 0.5, 1, 2$  and  $p = 15$  with fixed  $L = 10$ . The simulation results in second-, third- and fourth-row correspond to  $L = 5, 10$  and  $20$  respectively for  $p = L$  for sub-diffusive system at  $\alpha = 0.5$ , diffusive system at  $\alpha = 1$  and super-diffusive system at  $\alpha = 1.5$ .

## 6 Conclusion

In this article, we introduce Fourier spectral method that is capable of removing the stiffness issues associated with the higher-order spatial derivative of fractional reaction-diffusion systems. For the temporal discretization, we formulate fractional exponential integrator based on fourth order exponential time differencing to the resulting coupled system of ODEs in time. Mathematical analysis of notable two reaction-diffusion systems are conducted to give a clear definition of the parameter regimes. Simulations results of the fractional-in-space Schnakenberg and Gray-Scott models indicate that such equations can have some amazing dynamical patterns different from the standard reaction-diffusion. To explore the dynamic richness of spatial pattern formations, we experiment in both two and three dimensions for the sub-diffusive, diffusive and super-diffusive cases. It should be noted that the methodology presented in this work can be extended to multi-variable reaction-diffusion and fractional space-time reaction-diffusion systems.

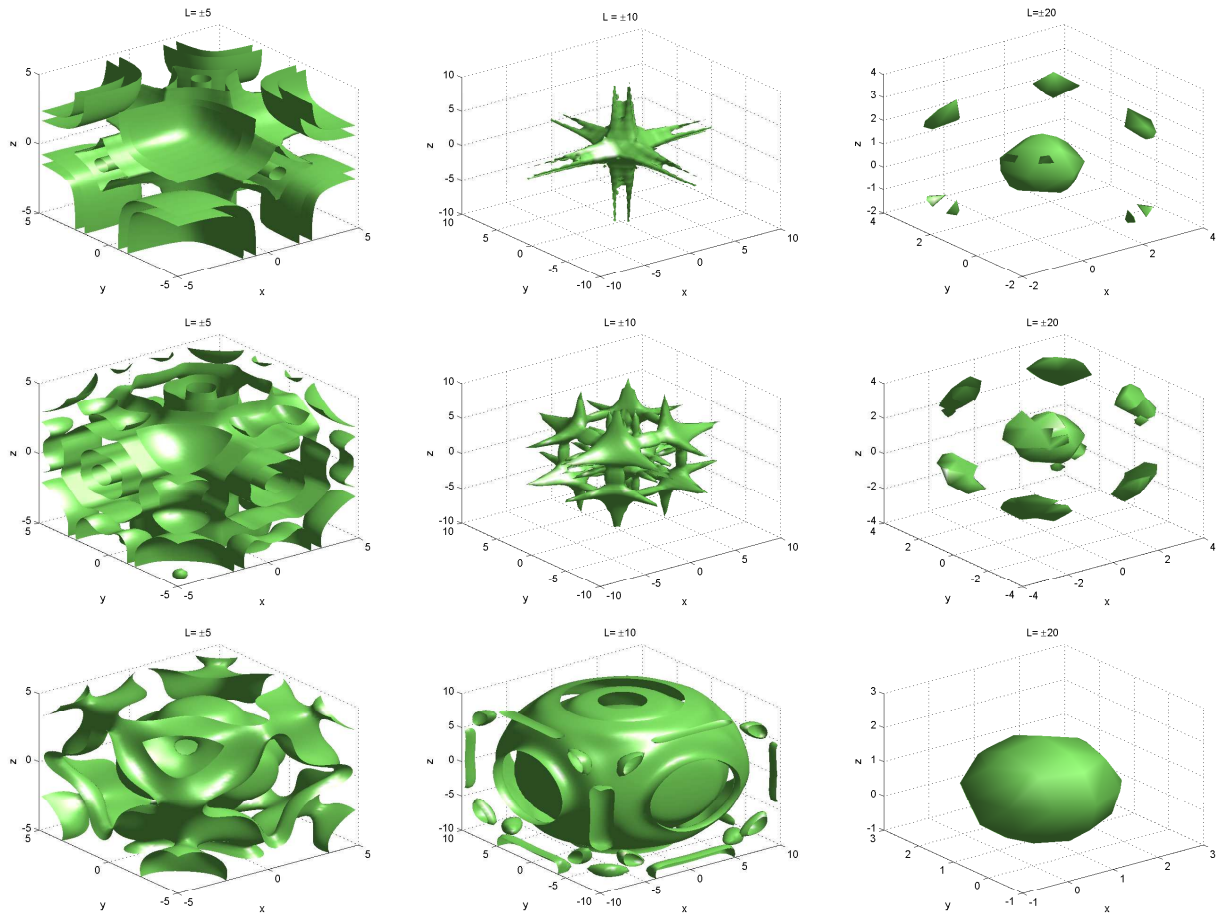


Figure 9: Snapshots of the evolution of substrate  $v$  for the Fractional reaction-diffusion system (58) in 3D obtained at instants of increasing domain  $[-L, L]$ , for  $L = 5, 10, 20$ . Upper-row shows the effect of pattern formation in sub-diffusive system with fractional power  $\alpha = 0.5$ . The middle-row indicates the patterns obtained for the normal reaction-diffusion at  $\alpha = 1$ . The lower-row corresponds to the super-diffusive system at  $\alpha = 1.5$ . Other parameters are as in Figure 8.

## References

- [1] Kilbas AA, Srivastava HM, Trujillo JJ. Theory and Applications of Fractional Differential Equations. New York: Elsevier; 2005.
- [2] Oldham KB, Spanier J. The Fractional Calculus. New York: Academic Press; 1974.
- [3] Podlubny I. Fractional Differential Equations, San Diego: Academic Press; 1999.
- [4] Carpinteri A, Mainardi F. Fractals and Fractional Calculus in Continuum Mechanics Vol.378 of CISM Courses and Lectures; Berlin: Springer-Verlag; 1997.
- [5] Hilfer E. Applications of Fractional Calculus in Physics. New York: World Sci. Publishing; 2000.

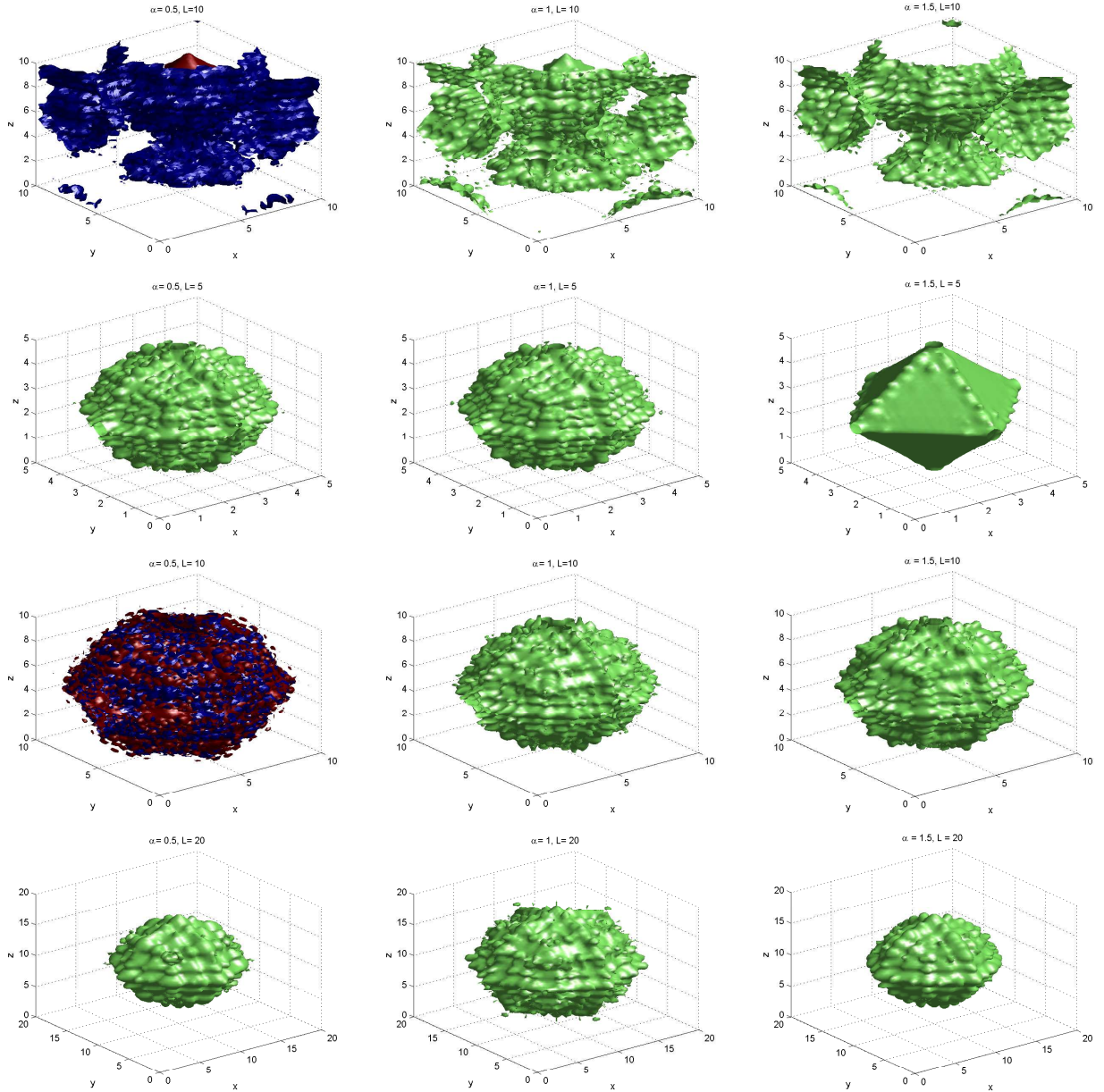


Figure 10: Three dimensional pattern formation in the fractional reaction-diffusion gray-Scott system (60) for different values of fractional power  $\alpha$  and domain size  $L$ . From the left, sub-diffusive results(first-column); diffusive (Second-column) and super-diffusive solutions (Third-column). Other parameters are:  $A = 9\epsilon$ ,  $B = 0.4\epsilon$ ,  $\epsilon = 0.005$ ,  $D_u = 2E - 5$  and  $D_v = 2D_u$  at final time  $t = 200$  with initial conditions (63).

- [6] Zaslavsky GM. Chaos and Fractional Dynamics. vol.511 of Lect. Notes in Phys. Oxford: Oxford University Press; 2005.
- [7] Chang FX, Wu JC, Dai SH. The fractional dispersion in pore medium and Lévy distribution. Journal of Nanjing University of Information Science and Technology, Natural Science Edition 2004;40(3):287-201.
- [8] Samko SG, Kilbas AA, Marichev OI. Fractional Integrals and Derivatives: Theory and

Applications. Amsterdam: Gordon and Breach; 1993.

- [9] Baeumer B, Meerschaert M, Benson D, Wheatcraft S. Subordinated advection-dispersion equation for contaminant transport. *Water Resour Res* 2001;37:1543-1550.
- [10] Zaslavsky G. Fractional kinetic equation for hamiltonian chaos, chaotic advection, tracer dynamics and turbulent dispersion. *Phys D* 1994;76 :110-122.
- [11] Raberto M, Scalas E, Mainardi F. Waiting-times and returns in high-frequency financial data: an empirical study. *Phys A* 2002;314:749-755.
- [12] Bai J, Feng XC. Fractional-order anisotropic diffusion for image denoising. *Image Process IEEE Trans* 2007;16:2492-2502.
- [13] Ariel PD. On a second parameter in the solution of the flow near a rotating disk by homotopy analysis method. *Commun Numer Anal* 2012;2012:1-13.
- [14] Panahipour H. Application of Extended Tanh Method to Generalized Burgers-type Equations. *Commun Numer Anal* 2012; 2012:1-14.
- [15] Keskin Y, Oturanc G. Reduced differential transform method: a new approach to fractional partial differential equations. *Nonli Sci Lett A* 2010;1:207-217.
- [16] Liu F, Anh V, Turner I, Zhuang P. Time fractional advection dispersion equation. *J Comput Appl Math* 2003;13:233-245.
- [17] Lin Y, Xu C. Finite difference/spectral approximations for the time-fractional diffusion equation. *J Comput Phys* 2007;225:1533-1552.
- [18] Holmes WR. An efficient, nonlinear stability analysis for detecting pattern formation in reaction diffusion systems. *Bull Math Biol* 2014;76: 157-183.
- [19] Murray JD. *Mathematical Biology II: Spatial Models and Biomedical Applications*. Berlin: Springer-Verlag; 2003.
- [20] Sander E, Wanner T. Unexpectedly linear behavior for the Cahn-Hilliard equation. *SIAM J Appl Math* 2000;60:2182-2202.
- [21] Sander E, Wanner T. Pattern formation in a nonlinear model for animal coats. *J Differ Equ* 2002;191:143-174.
- [22] Gray P, Scott SK. Autocatalytic reactions in the isothermal, continuous stirred tank reactor: isolas and other forms of multistability. *Chem. Eng. Sci.* 1983;38:29-43.
- [23] Gray P, Scott SK. Autocatalytic reactions in the isothermal, continuous stirred tank reactor: oscillations and instabilities in the system  $A + 2B \rightarrow 3B, B \rightarrow C$ . *Chem. Eng. Sci.* 1984;39:1087-1097.
- [24] Gray P, Scott SK. Sustained oscillations and other exotic patterns of behavior in isothermal reactions. *J. Phys. Chem.* 1995;89:22-32.

- [25] Munteanu A, Sole RV. Pattern formation in noisy self-replicating spots. *Inter J Bifur Chaos* 2006;16: 3679.
- [26] Owolabi KM. Robust IMEX schemes for solving two-dimensional reaction-diffusion models. *Inter J Nonlin Sci Numer Simul* 2015;16:271-284.
- [27] Doelman A. Kaper TJ, Zegeling PA. Pattern formation in the one-dimensional Gray-Scott model. *J. Nonlin Sci* 1997;10:523-563.
- [28] Muratov CB, Osipov VV. Spike autosolitons and pattern formation scenarios in the two-dimensional Gray-Scott model. *Eur Phys J B* 2001;22:213-221.
- [29] Muratov CB, Osipov VV. Stability of the static spike autosolitons in the two-dimensional Gray-Scott model. *SIAM J Appl Math* 2002;62:1463-1487.
- [30] Garvie M. Finite-difference schemes for reaction-diffusion equations modeling predator-prey interactions in MATLAB. *Bull Math Biol* 2007;69:931-956.
- [31] Garvie M, Trenchea C. Spatiotemporal dynamics of two generic predator-prey models. *J Biol Dyn* 2010;4:559-570.
- [32] Sun G, Zhang G, Jin Z, Li L. Predator cannibalisms can give rise to regular spatial patterns in a predator-prey system. *Nonlin Dyn* 2009;58:75-84.
- [33] Owolabi KM, Patidar KC. Existence and permanence in a diffusive KiSS model with robust numerical simulations. *Inter J Differ Equ* (2015);2015(485860):8. doi:10.1155/2015/485860.
- [34] Trefethen LN. *Spectral Methods in MATLAB*. Philadelphia: SIAM; 2000.
- [35] Cox SM, Matthews PC. Exponential time differencing for stiff systems. *J Comput Phys* 2002;176:430-455.
- [36] Kassam AK, Trefethen LN. Fourth-order time stepping for stiff PDEs. *SIAM J Sci Comput* 2005; 26:1214-1233.
- [37] Owolabi KM, Patidar KC. Numerical simulations of multicomponent ecological models with adaptive methods. *Theor Biol Med Model* 2016;13:1. DOI 10.1186/s12976-016-0027-4.
- [38] Owolabi KM, Patidar KC. Effect of spatial configuration of an extended nonlinear Kierstead-Slobodkin reaction-transport model with adaptive numerical scheme. *Springer Plus* 2016;5:303. DOI 10.1186/s40064-016-1941-y
- [39] Munthe-Kaas H. High order Runge-Kutta methods on manifolds. *Appl Numer Math* 1999;29:115-127.
- [40] Owolabi KM, Patidar KC. Higher-order time-stepping methods for time-dependent reaction-diffusion equations arising in biology. *Appl Math Comput* 2014;240:30-50.
- [41] Owolabi KM, Patidar KC. Numerical solution of singular patterns in one-dimensional Gray-Scott-like models. *Inter J Nonlin Sci Numer Simul* 2014;15:437-462.

- [42] Doelman A, Gardner RA, Kaper TJ. Stability analysis of singular patterns in the 1d GS model: a matched asymptotic approach. *Phys D Nonlin Phenom* 1998;122:1-36.